Metal-free organic sensitizers for use in water-splitting dye-sensitized photoelectrochemical cells

John R. Swierk[a], Dalvin D. Méndez-Hernández[b], Nicholas S. McCool[a], Paul Liddell[b], Yuichi Terazono[b], Ian Pahk[b], John J. Tomlin[b], Nolan V. Oster[b], Thomas A. Moore[b], Ana L. Moore[b], Devens Gust[b], and Thomas E. Mallouk[a,c,1]

Departments of [a]Chemistry and [c]Biochemistry and Molecular Biology, Pennsylvania State University, University Park, PA 16802; and [b]Department of Chemistry and Biochemistry and Center for Bio-Inspired Solar Fuel Production, Arizona State University, Tempe, AZ 85287

Edited by Richard Eisenberg, University of Rochester, Rochester, NY, and approved December 12, 2014 (received for review August 4, 2014)

Solar fuel generation requires the efficient capture and conversion of visible light. In both natural and artificial systems, molecular sensitizers can be tuned to capture, convert, and transfer visible light energy. We demonstrate that a series of metal-free porphyrins can drive photoelectrochemical water splitting under broadband and red light ($\lambda > 590$ nm) illumination in a dye-sensitized TiO_2 solar cell. We report the synthesis, spectral, and electrochemical properties of the sensitizers. Despite slow recombination of photoinjected electrons with oxidized porphyrins, photocurrents are low because of low injection yields and slow electron self-exchange between oxidized porphyrins. The free-base porphyrins are stable under conditions of water photoelectrolysis and in some cases photovoltages in excess of 1 V are observed.

water-splitting | photoelectrochemical | metal-free porphyrins | visible light | artificial photosynthesis

The capture of solar energy and storage as reduced chemical fuels is a significant challenge for a future renewable energy economy. Solar fuels may take the form of H_2 or reduced carbon-containing molecules (CH_4, C_2H_6, CH_3OH, etc.). Large-scale reduction of water or CO_2 requires an abundant electron donor to provide the reducing equivalents. Natural photosynthesis uses water as the electron source, generating oxygen as a byproduct. Most artificial photosynthetic systems also seek to use water as the electron donor, even though the kinetically slow oxygen evolution step is a performance bottleneck (1).

The thermodynamic requirements for water oxidation are relatively modest. A minimum potential of 1.23 V is required, although practical systems need higher voltages because of catalytic overpotentials and series losses in photoelectrolysis cells. This minimum thermodynamic requirement can be satisfied by light of all wavelengths shorter than 1 μm. Allowing for reasonable overpotentials and series losses, the minimum onset for light absorption in a one-photon-per-electron system is near 650 nm, and the maximum theoretical power conversion efficiency is about 20% (2). Although many molecular sensitizers and solid-state semiconductors absorb in this range, finding stable sensitizers with redox or band potentials that span the water oxidation and reduction potentials is a significant challenge.

Light harvesting in natural photosynthesis is accomplished by a hierarchical assembly of accessory pigments that funnel their excitation energy to chlorophyll molecules (3). The core of chlorophyll-*a* is a substituted chlorin (4), a porphyrin ring with a reduced exo double bond (5). Because porphyrins are synthetically more accessible than chlorins and bacteriochlorins, many groups have studied them as light-harvesting molecules in dye-sensitized solar cells (DSSCs) (6, 7). Unlike ruthenium polypyridyl dyes, porphyrins contain only abundant elements and strongly absorb across most of the visible spectrum (8). Grätzel and coworkers recently demonstrated a 12.3% efficient DSSC for electricity generation, using a push–pull Zn porphyrin (9).

In contrast to conventional DSSCs, water-splitting dye-sensitized photoelectrochemical cells (WS-DSPECs) use molecular sensitizers and water oxidation catalysts that are coadsorbed onto a mesoporous TiO_2 electrode. The sensitizer absorbs visible light, injects an electron into the conduction band of TiO_2, and is then re-reduced by the water oxidation catalyst, which oxidizes water to give molecular oxygen and protons. The photoinjected electron migrates through the TiO_2 film to a dark cathode where protons are reduced to molecular hydrogen (1). At high light intensity in the blue part of the visible spectrum, incident photon current efficiencies (IPCEs) up to 14% have been demonstrated with WS-DSPECs (10).

Earth-abundant catalysts and sensitizers will be needed for large-scale deployment of artificial photosynthesis. Much effort has been devoted to the development of earth-abundant water oxidation catalysts (11–14), including a recently reported completely organic catalyst (15). Less attention has been paid to the development of earth-abundant sensitizers—an important problem for WS-DSPECs where absorber-to-catalyst ratios can exceed 1,000:1. Ruthenium polypyridyl sensitizers are most commonly used in WS-DSPECs (10, 16–19), although Moore et al. (20) demonstrated a WS-DSPEC sensitized with a zinc porphyrin that produced modest photocurrent (~30 μA/cm^2). Organic sensitizers (containing C, H, N, and O) are earth abundant and offer the possibility of being low cost. The viability of organic sensitizers has been studied in conventional DSSCs (21, 22) and organic solar cells (23, 24), but is largely unexplored in the context of water splitting. Tachan et al. recently proposed type II sensitization with catechol on TiO_2 (25). They observed current enhancement, although the Faradaic efficiency of oxygen

Significance

The capture and conversion of sunlight into a useful chemical fuel (H_2, CH_4, CH_3OH, etc.) is a central goal of the field of artificial photosynthesis. Water oxidation to generate O_2 and protons stands as the major bottleneck in these processes. Relatively few stable photosensitizers can generate sufficient oxidizing power to drive water oxidation, and those that do contain rare elements such as ruthenium. In this paper, we show that metal-free organic photosensitizers are capable of driving photoelectrochemical water oxidation. Significantly, these photosensitizers exhibit comparable activity to that of ruthenium-containing photosensitizers under broadband illumination. In addition, we report to our knowledge the first demonstration of a molecular photosensitizer, outside of natural photosynthesis, that can drive water oxidation utilizing only red light.

Author contributions: J.R.S., D.D.M.-H., T.A.M., A.L.M., D.G., and T.E.M. designed research; J.R.S., D.D.M.-H., N.S.M., P.L., Y.T., I.P., J.J.T., and N.V.O. performed research; J.R.S., D.D.M.-H., N.S.M., P.L., Y.T., I.P., J.J.T., N.V.O., T.A.M., A.L.M., D.G., and T.E.M. analyzed data; and J.R.S. and D.D.M.-H. wrote the paper.

The authors declare no conflict of interest.

This article is a PNAS Direct Submission.

[1]To whom correspondence should be addressed. Email: tem5@psu.edu.

This article contains supporting information online at www.pnas.org/lookup/suppl/doi:10.1073/pnas.1414901112/-/DCSupplemental.

generation was not measured and it is unclear how much of the enhancement was specific to visible light sensitization.

In this paper, we demonstrate overall water splitting using metal-free organic sensitizers. We show that a series of free-base porphyrins can drive the photoelectrochemical water-splitting reaction, using only visible light illumination at photocurrents comparable to those of Ru polypyridyl sensitizers. TiO_2 electrodes sensitized with these porphyrins generate photocurrent corresponding to water oxidation, even when illuminated with red light ($\lambda > 590$ nm). Although hole transport and injection yields are poor, back electron transfer recombination is much slower than it is with the most widely used Ru polypyridyl sensitizer.

Methods

Detailed syntheses and characterization data for the compounds used in this study, along with additional details of the photoelectrochemical experiments, can be found in *SI Appendix*.

Preparation of WS-DSPEC Electrodes. IrO_2-catalyzed TiO_2 photoanodes were made as described elsewhere (19). An aqueous paste of anatase TiO_2 nanoparticles was applied to an 8-Ω/cm^2 fluorine-doped tin oxide-coated glass slide via a doctor blading technique. After sintering, the electrodes were soaked in 100 μM citrate-capped IrO_x solution for 14 h and then sintered for 3 h at 450 °C to form crystalline IrO_2. Electrical contact was made with a conducting silver paste and protected with Hysol C Loctite white epoxy. The electrodes were then soaked in a 200-μM solution of sensitizer in ethyl acetate for 22 h in the dark, rinsed with fresh ethyl acetate, and stored in the dark.

Characterization of Electrodes. Sensitizer surface coverages on TiO_2 were determined using the Q-band absorbance in solution and on dry TiO_2 films. Emission data were collected on TiO_2 coated with an insulating ZrO_2 shell applied by atomic layer deposition (ALD) via excitation of the $Q_y(1,0)$ peak. Photoelectrochemical measurements were made using a 150-W Xe lamp fitted with air mass (AM) 0, AM 1.5, and 410-nm or 590-nm long-pass filters, which prevented band gap excitation of the TiO_2. Short-circuit absorbed photon-to-current efficiency (APCE) measurements were made with a Metrohm Autolab potentiostat with a 1-ms time resolution. A 470-nm light-emitting diode (LED) (Thorlabs M470L3) was used as the illumination source. Open-circuit photovoltage decay measurements also used the 470-nm LED to provide bias illumination, with a 532-nm pulse (5 mJ, 7–10 ns) from a Nd:YAG laser (SpectraPhysics INDI-40-10) used to pump the system. The voltage decay was monitored on an oscilloscope (Tektronix TDS 540A). The current efficiency for oxygen generation at the photoanodes was measured using a calibrated Pt collector electrode as previously described (18, 19). For each value reported, standard errors were calculated from measurements of six replicate samples. Detailed characterization procedures are reported in *SI Appendix*.

Results

Absorption and Emission Spectra. Free-base porphyrins exhibit a strong Soret band absorption in the near-UV/blue portion of the spectrum and four lower-intensity Q bands at longer wavelengths (26). The Soret bands for the sensitizers studied in this work (Fig. 1) typically had maxima at ~410 nm, with extinction coefficients in excess of 10^5 $M^{-1}\cdot cm^{-1}$. As the light source used for photoelectrochemical measurements is equipped with a 410-nm long-pass filter, it is the Q bands of the sensitizers that are of particular importance in this study. *SI Appendix*, Table S1 gives the absorbance maxima and molar extinction coefficients for the Q bands of each sensitizer.

An analysis of the absorbance maxima in *SI Appendix*, Table S1 shows that the position of the Q bands is influenced by the type and number of substituents at the meso positions of the porphyrin ring. TMP, TTP, and PAP have alkylphenyl substituents at each meso position and have nearly identical absorbance maxima. The MMP, DMP, and TMP series exhibits a 6- to 8-nm red shift with each additional mesityl group. With MDC and MDCE, the four Q bands appear at nearly identical positions. Molar extinction coefficients also show some general trends, with fully substituted porphyrins generally having larger values. On the dry, sensitized TiO_2 films, the positions of the Q bands show a slight red shift (~1–3 nm) (*SI Appendix*, Table S2). Typically, the absorbance at the $Q_y(1,0)$ peak was between 1 and 2 absorbance units, with the subsequent Q bands following the trends in extinction coefficient measured in solution. The surface coverage (*SI Appendix*, Table S2) was calculated using the absorbance of the $Q_y(1,0)$ maximum.

The fluorescence spectra of the porphyrin sensitizers contained two well-defined peaks, the higher-energy emission assigned to the Q(0,0) transition and the lower-energy one assigned to Q(1,0) (Table 1). As in the absorption spectra, the emission maxima shifted to the red as the number of meso-mesityl groups increased from MMP to TMP (*SI Appendix*, Fig. S1). For the fully substituted sensitizers (TMP, TTP, and PAP), the position of the Q(1,0) fluorescence peak was consistent; however, for TTP the Q(0,0) peak (663 nm) was shifted 9 nm to the red relative to TMP and PAP (654 nm). These porphyrins, as well as DMEP, show a mirror image relationship in the relative intensities of the Q(0,0) and Q(1,0) absorption and emission bands.

Electrochemistry. The peak of the anodic wave (E_{pa}) for the sensitizers on TiO_2 is presented in Table 1. MDC is not included as it rapidly desorbed during the experiment. We determined E_{pa} by cyclic voltammetry (*SI Appendix*, Fig. S2). On TiO_2 the oxidation of the sensitizers was electrochemically irreversible, as previously reported (20). The trends in E_{pa} differed from the observed spectral trends. For example, increasing the number of mesityl substituents introduces a very slight positive shift in E_{pa}, while exerting a more significant effect on the spectral properties. The E_{pa} value for TMP is in close agreement with the value (1.09 V vs. Ag/AgCl) measured by Watson et al. (27). Although

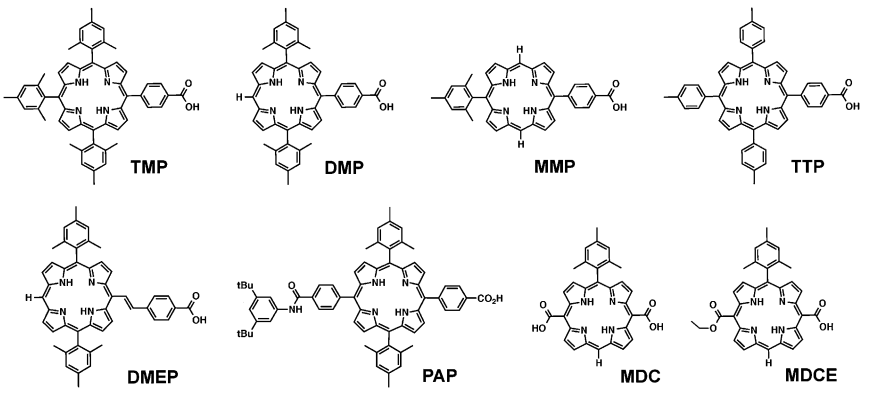

Fig. 1. Free-base porphyrin sensitizers used in this study. Compound acronyms are defined in *SI Appendix*.

Table 1. Emission maxima (nm), singlet energy gap (eV), ground-state peak of anodic wave (E_{pa}), and excited-state reduction potentials (E^*_{red}) (V vs. Ag/AgCl) of sensitizers

Porphyrin	Q(0,0)†	Q(0,1)†	E(0,0)	E_{pa}	E^*_{red}
TMP	654 (1.0)	721 (0.9)	1.91	1.05	−0.86
DMP	645 (1.0)	710 (1.6)	1.94	1.04	−0.90
MMP	641 (1.0)	702 (1.5)	1.96	1.02	−0.94
DMEP	683 (1.0)	738 (0.6)	1.87	1.18	−0.67
TTP	663 (1.0)	721 (0.8)	1.90	1.18	−0.72
PAP	655 (1.0)	720 (0.8)	1.91	1.29	−0.62
MDCE	677 (1.0)	700 (1.1)	1.92	1.03	−0.89

†Relative intensity of the peaks is in parentheses.

TMP, TTP, and PAP have similar spectral characteristics, their E_{pa} values are markedly different, with TMP and PAP separated by 240 mV (*SI Appendix*, Fig. S2).

The excited-state reduction potential E^*_{red} was estimated as the difference between E_{pa} of the ground state and the lowest-energy singlet (E_{00}), determined by the crossing point of the normalized emission and absorption spectra. The porphyrins studied had very similar E_{00} values, so E^*_{red} was largely determined by the position of E_{pa}. E^*_{red} has direct implications for the ability of the excited sensitizer to inject an electron into in the conduction band of TiO_2. For anatase, the conduction band edge potential is about −0.81 V vs. Ag/AgCl at pH 6.8 (28).

In addition to absorbing visible light, the sensitizer must also conduct holes across the surface to a catalytic IrO_2 particle. Intermolecular hole transfer between sensitizers on TiO_2 has been well studied in the context of conventional DSSCs (29–31). Focusing on sensitizers relevant to WS-DSPECs, Hanson et al. (32) measured the cross-surface electron diffusion coefficients (D_{app}) for a series of ruthenium polypyridyl complexes by polarizing the electrode positive of their formal potential and then monitoring the bleaching of the metal-to-ligand charge transfer (MLCT) absorbance. The absorbance-time curve was fitted to a modified Cottrell equation to give the apparent cross-surface electron diffusion coefficient. Using the same method, we found that D_{app} for the porphyrin sensitizers used in this study was too slow to measure ($\leq 10^{-11}$ $cm^2 \cdot s^{-1}$). By comparison, ruthenium polypyridyl complexes typically have D_{app} values on the order of 10^{-9}–10^{-11} $cm^2 \cdot s^{-1}$ (32, 33).

Photoelectrochemistry. For WS-DSPECs, the photovoltage is defined as the difference between the potential of water oxidation (+0.63 V vs. Ag/AgCl at pH 6.8) and the Fermi level of the TiO_2 under illumination (19). We previously determined the optimal IrO_2 loading to be 0.5 pmol/cm^2 (19). At this loading, we measured open-circuit photovoltages of 1.07 ± 0.01 V and 1.11 ± 0.03 V with the $[Ru(bpy)_2(4,4'\text{-}(PO_3H_2)_2bpy)]$ sensitizer (19, 33). The photovoltages we observed in this study were generally similar and fell between 1.00 V and 1.10 V (Table 2). MDC exhibited a significantly lower photovoltage (0.88 ± 0.01 V); however, it desorbed from the TiO_2 at a significant rate under illumination (*SI Appendix*, Fig. S4). Under red light illumination (AM 1.5 simulated solar spectrum with a 590-nm long-pass filter), a photovoltage drop of ∼0.10 V was observed.

We measured the photocurrent at +0.10 V vs. Ag/AgCl applied bias for 10 min under illumination. For ready comparison between sensitizers, we integrated the current to find the charged passed (*SI Appendix*, Fig. S3). For the majority of sensitizers there was little difference in the integrated charge under illumination with a 410-nm long-pass filter (Table 1). PAP and DMP were notable exceptions, passing about half the charge of the other sensitizers. Integrating the photon flux from 410 nm to 700 nm, we calculated IPCE values of 0.014–0.032% for the 10 min of illumination. Under red light (590-nm long-pass filter), the charge passed decreased although IPCE values generally remained constant. Samples that lacked sensitizer or IrO_2 showed no measurable photocurrent (<1 $\mu A \cdot cm^{-2}$) with either the 410-nm or the 590-nm long-pass filter. A small transient current that decays within 100 ms can be observed when a sensitizer is present but no IrO_2 is present.

We determined the Coulombic efficiency for oxygen evolution of a TMP-sensitized photoanode (Fig. 2), as previously described (18, 19). When the cell was degassed with Ar, the collector electrode showed a small cathodic background current (∼60 μA) before illumination. Once the cell was exposed to light, the photoanode generated photocurrent that was mirrored in time on the collector electrode. Using the collection efficiency (81%) determined by calibration with a Pt film generator electrode, we calculated a Faradaic efficiency of 102 ± 5%, (i.e., near unity) for water oxidation at the WS-DSPEC photoanode.

To better understand the IPCE values of the various sensitizers on TiO_2, we sought to measure the quantum yield of injection. Meyer and coworkers (34) used a poly(methylmethacrylate) actinometer to measure quantum yields for injection of electrons from excited ruthenium polypyridyl dyes into TiO_2; however, we were unable to accurately determine the molar extinction coefficient of the porphyrin radical cation following injection. Thus, instead of directly determining the injection yield, we measured the APCE under short-circuit conditions. Electrodes with 4-μm-thick TiO_2 films were used to promote efficient charge collection. These films were not functionalized with catalyst, so the APCE was calculated from the photocurrent in the first millisecond of illumination in pH 6.8, 100-mM phosphate buffer. To minimize recombination effects the system was held at short circuit and the measurement was performed over a short time period (1 ms). $[Ru(bpy)_2(4,4'\text{-}(PO_3H_2)_2bpy)]$ was used as a comparison sensitizer, as quantum yields for injection by ruthenium polypyridyl sensitizers are typically high. Table 3 reports the short-circuit APCE values for the sensitizers. Surprisingly, the APCE values in the TMP, DMP, and

Table 2. Photoelectrochemical data for various sensitizers, open-circuit voltage (mV), integrated photocurrent ($mC \cdot cm^{-2}$), and incident photon current efficiency (IPCE)

	410 nm long-pass			590 nm long-pass		
Porphyrin	V_{oc}	Integrated photocurrent	IPCE, %	V_{oc}	Integrated photocurrent	IPCE, %
TMP	1,045 ± 5	5.1 ± 0.1	0.028 ± 0.005	909 ± 21	0.8 ± 0.0	0.009 ± 0.001
DMP	1,088 ± 5	3.7 ± 0.9	0.018 ± 0.005	1,004 ± 7	2.5 ± 0.2	0.029 ± 0.002
MMP	1,054 ± 17	6.4 ± 0.6	0.032 ± 0.003	910 ± 5	1.6 ± 0.3	0.018 ± 0.003
DMEP	1,020 ± 15	7.2 ± 1.5	0.036 ± 0.007	945 ± 16	1.6 ± 0.5	0.019 ± 0.006
TTP	1,080 ± 4	5.7 ± 1.0	0.028 ± 0.005	953 ± 12	2.5 ± 0.2	0.030 ± 0.006
PAP	1,008 ± 15	2.8 ± 0.8	0.014 ± 0.004	878 ± 15	1.0 ± 0.0	0.011 ± 0.001
MDC	879 ± 12	0.5 ± 0.0	0.006 ± 0.000	700 ± 12	0.1 ± 0.0	0.001 ± 0.000
MDCE	1,078 ± 7	6.6 ± 0.3	0.032 ± 0.002	982 ± 14	2.2 ± 0.0	0.025 ± 0.000

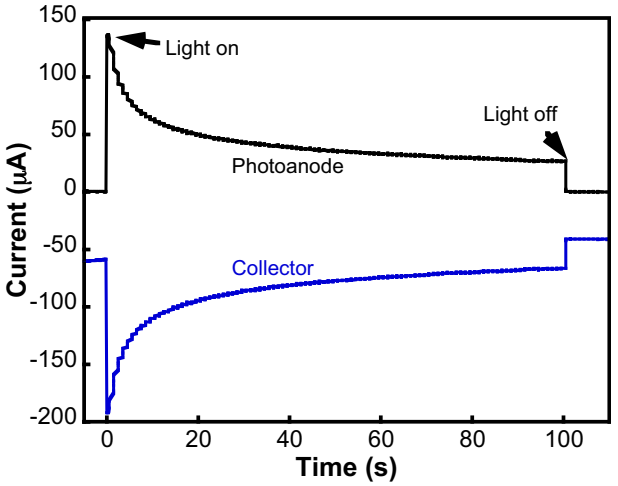

Fig. 2. Collector–generator experiment to monitor O_2 Faradaic efficiency. The generator electrode is a TMP-sensitized photoanode at +100 mV vs. Ag/AgCl, and the collector electrode is a planar Pt film at −640 mV vs. Ag/AgCl (3 M NaCl). Faradaic efficiency is calculated as ∼100%, and collection efficiency previously determined is 81%.

MMP series were in the reverse order of the overpotential for charge injection. PAP had the lowest APCE value (2.4 ± 0.2%), consistent with its more positive excited-state reduction potential. By contrast, $[Ru(bpy)_2(4,4'\text{-}(PO_3H_2)_2bpy)]$ had an APCE 3–10 times higher than that of the porphyrin sensitizers.

We also compared the transient open-circuit photovoltage decay rates for each sensitizer and $[Ru(bpy)_2(4,4'\text{-}(PO_3H_2)_2bpy)]$ (Table 3). Photovoltage decay curves were fitted to a stretched exponential function to extract the recombination time constant, τ_r (Fig. 3). For the porphyrin sensitizers, values of τ_r were on the order of tens of milliseconds, with some correlation between longer recombination time and the number of substituents. Interestingly, the porphyrins exhibited a τ_r roughly one order of magnitude longer than that of $[Ru(bpy)_2(4,4'\text{-}(PO_3H_2)_2bpy)]$. It is important to note that illumination intensity and not V_{oc} was kept constant for each sensitizer, although V_{oc} values were consistent with values measured under broadband illumination.

Discussion

The open-circuit photovoltages and integrated photocurrents are quite similar for most of the free-base porphyrin sensitizers. However, a deeper analysis of the spectral and electrochemical properties of the sensitizers reveals significant differences. To properly understand the photoelectrochemical results, it is crucial to understand these differences and to develop a kinetic picture so we can rationally design strategies to improve the system.

Analysis of the spectral and electrochemical data reveals that these properties are directly affected by substitution on the porphyrin core. Symmetry, inductive, and resonance effects may cause these differences. We can observe the effect of symmetry if we compare TMP, DMP, and MMP. Generally, the four-orbital model is used to describe the absorption spectra of porphyrins (26, 35). With free-base porphyrins, the N-H protons on the pyrrole core reduce the overall symmetry of the molecule and split the Q bands into Q_x and Q_y components. This band splitting functionally extends the absorption into the red. Substitution at the meso position shifts the energy of one highest occupied molecular orbital (HOMO) and both lowest unoccupied molecular orbitals (LUMOs). The other HOMO orbital has a nodal plane at the meso position and is unaffected (26). With each additional mesityl group, the molecule becomes more symmetric electronically, the Q bands shift by 6–8 nm to the red, and the molar extinction coefficients increase. Although TMP does not strictly have D_{4h} symmetry, we assume that the aryl groups at each meso position give it quasi-D_{4h} symmetry.

Porphyrin electrochemistry is classically described by the Hammett linear free energy relationship, with the potential of the radical π cation sensitive to the inductive electron donating/withdrawing character of the substituent and the stabilizing/destabilizing character of any π bonds (36). Inductive effects in this study are hard to elucidate as mesityl, tolyl, and hydrogen are electron-donating groups (36). Resonance between aryl substituents and the π system of the macrocycle core in this study would be expected to stabilize the radical cation.

Resonance stabilization effects can be clearly seen when comparing TMP, TTP, and PAP. From a symmetry standpoint, these compounds are similar with aryl groups at each meso position; the similarity in Q-band absorbance maxima reflects this shared symmetry. Additionally, the inductive effects of the substituents are expected to be similar (36). We might expect TMP to have the least resonance stabilization as steric effects between mesityl and the macrocycle core typically result in a dihedral angle close to 90°. In contrast the aryl groups on TTP and PAP are less hindered and closer to coplanarity with the porphyrin core, thus allowing resonance stabilization effects to cathodically shift E_{pa}. Surprisingly, we see an anodic shift in E_{pa} for TTP and PAP, with TTP shifted by 130 mV and PAP by 240 mV relative to TMP. McLendon and coworkers offer a possible explanation for this behavior (37). In bridged porphyrin adducts, they observe maximum rates of intramolecular electron transfer at 0° and 90°, with the minimum rate near 45°. They attribute this result to orbital symmetry considerations. As we noted, mesityl groups exhibit dihedral angles of ∼90°, whereas tolyl groups sit at an angle closer to 60° (38).

The combined effects of substitution on the spectral and electrochemical properties of the porphyrins are reflected in the excited-state reduction potential, E^*_{red}. A sensitizer with an E^*_{red} that is too positive will have low yields of electron injection into TiO_2. Thus, more efficient cells should incorporate sensitizers that have resonance stabilization and cathodically shifted E_{pa}. However, the picture is more complicated. For example, the excited-state reduction potential of TTP is 220 mV more positive than that of MMP, yet within error both sensitizers generate the same amount of integrated photocurrent. Part of this is certainly related to differences in E_{pa}. The E_{pa} of TTP is 160 mV more positive than that of MMP and the former should exhibit a more rapid rate of electron transfer from the IrO_2 catalyst. It is important to be cautious about shifting the potential of the radical cation too positive as PAP demonstrates. Despite being the most strongly oxidizing of the sensitizers tested, E^*_{red} for PAP is too positive for efficient injection into TiO_2 as the APCE results indicate. The overall effect leads to low photocurrent.

We would expect that the wider coverage of the visible spectrum by free-base porphyrin sensitizers would lead to higher photocurrents relative to $[Ru(bpy)_2(4,4'\text{-}(PO_3H_2)_2bpy)]$. In fact, we see the opposite: Porphyrin-modified electrodes generated roughly half

Table 3. Short-circuit absorbed photon-to-current efficiency (APCE) and open-circuit photovoltage decay time (ms)

Porphyrin	APCE	τ_r	β
TMP	0.074 ± 0.011	59 ± 5	0.52 ± 0.11
DMP	0.066 ± 0.005	29 ± 6	0.56 ± 0.02
MMP	0.031 ± 0.004	25 ± 2	0.54 ± 0.04
DMEP	0.044 ± 0.002	30 ± 4	0.43 ± 0.02
TTP	0.052 ± 0.017	38 ± 1	0.52 ± 0.13
PAP	0.024 ± 0.002	33 ± 1	0.50 ± 0.03
MDCE	0.038 ± 0.006	59 ± 2	0.49 ± 0.02
$[Ru(bpy)_2(4,4'\text{-}(PO_3H_2)_2bpy)]$	0.209 ± 0.017	4 ± 1	0.47 ± 0.01

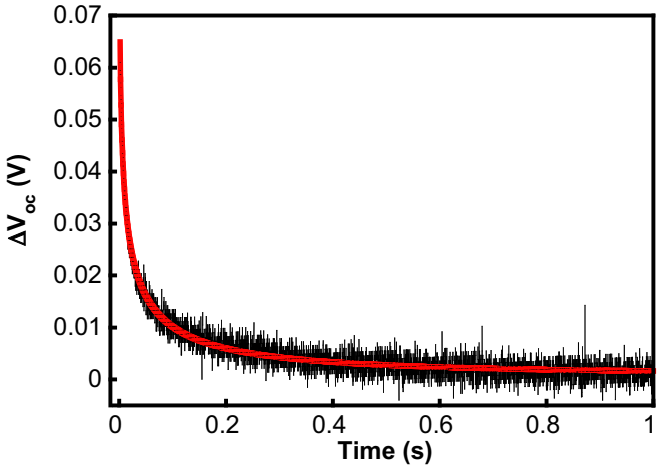

Fig. 3. Representative transient open-circuit photovoltage decay for a DMP-sensitized electrode. Steady-state bias was provided by a 470-nm LED and the pump was generated by a 532-nm ND:YAG laser pulse (t = 0). Red line, fit to $\Delta V_{oc} = \Delta V_{oc,0} \exp[(\tau/t)^{\beta}]$.

the photocurrent of analogous $[Ru(bpy)_2(4,4'\text{-}(PO_3H_2)_2bpy)]$ cells. As a starting point to understand this difference, we first consider surface coverage. $[Ru(bpy)_2(4,4'\text{-}(PO_3H_2)_2bpy)]$ has a surface coverage on the order of 1×10^{-7} mol/cm^2 (33). In the current study, the bulky sensitizers TMP and PAP had the lowest surface coverages (0.45×10^{-7} mol/cm^2 and 0.42×10^{-7} mol/cm^2); however, TTP exhibited a higher surface coverage, possibly because the tolyl groups can achieve greater planarity, and the lack of ortho-methyl groups would allow closer approach of the macrocycles. MDC exhibited a high surface coverage relative to MDCE (0.61×10^{-7} mol/cm^2), possibly due to electrostatic effects. An increase in surface coverage is observed in going from TMP to DMP (0.92×10^{-7} mol/cm^2) with a very significant increase in coverage observed with MMP (2.8×10^{-7} mol/cm^2). Steric effects are probably at work in this case. With every sensitizer the surface coverage is comparable to typical $[Ru(bpy)_2(4,4'\text{-}(PO_3H_2)_2bpy)]$ coverages and thus the coverage trends cannot explain the differences in photocurrent.

A second possibility is that the porphyrin sensitizers are not electrochemically stable. As noted above, the oxidation of the sensitizers on TiO_2 is electrochemically irreversible, which could indicate a side reaction of the radical cation or desorption of the oxidized species from the electrode. Several lines of evidence argue for photoelectrochemical stability and authentic water oxidation activity. First, as noted above, irreversibility of porphyrins on TiO_2 has been previously observed (20). Also, we have observed that films of $[Ru(bpy)_2(4,4'\text{-}(PO_3H_2)_2bpy)]$ with poor hole transport characteristics also exhibit electrochemical irreversibility on TiO_2 (33). Second, in nonaqueous solutions TMP (27) and TTP (39) are reversible, suggesting that the irreversibility we observe is not due to fundamental chemical instability of the sensitizers. Third, UV-Vis spectra of the electrodes before and after photoelectrolysis generally show no change in absorption, except for MDC (*SI Appendix*, Fig. S4). If the sensitizers are unstable, we would expect to see a change both in peak absorbances and in the shape of the absorption spectrum. Although we do see some increase in absorbance after electrolysis, we suggest that this is related to residual water within the mesoporous TiO_2 and not to sensitizer modification. Finally, we directly observe oxygen generation and determine a Faradaic efficiency close to 100%.

As surface coverages, electrochemical stabilities, and excited-state potentials of these sensitizers are comparable to those of $[Ru(bpy)_2(4,4'\text{-}(PO_3H_2)_2bpy)]$, we identify two major differences: injection into TiO_2 and cross-surface hole transport (Fig. 4). Although we do not directly measure a quantum yield of injection, the APCE for $[Ru(bpy)_2(4,4'\text{-}(PO_3H_2)_2bpy)]$ is 3–10 times larger than APCEs of the porphyrin sensitizers. For some of the porphyrin sensitizers, E^*_{red} is positive of the conduction band edge potential of TiO_2. From that perspective it is surprising that some sensitizers, PAP for example, inject into TiO_2. In this case, it is possible that hot injection may occur from the higher-energy Q(1,0) transitions (40). Under 590-nm long-pass illumination, only a portion of the $Q_y(1,0)$ band is typically illuminated, which could allow for hot injection. Also, fast deactivation pathways may contribute to poor injection. Finally, the anchoring group can have an important effect on electron injection (41, 42). This likely can explain the high photocurrents observed for DMEP and MDCE. In these two molecules, the orbital overlap between the porphyrin macrocycle and the carboxyl group is not impeded by a large dihedral angle between the macrocycle and a meso phenyl ring, as it is in the other compounds.

The other significant difference we observe compared with $[Ru(bpy)_2(4,4'\text{-}(PO_3H_2)_2bpy)]$ electrodes is hole transport by the sensitizer layer. For $[Ru(bpy)_2(4,4'\text{-}(PO_3H_2)_2bpy)]$ at a surface coverage of 10^{-7} mol·cm^{-2}, typical values for D_{app} are in the range of 10^{-9}–10^{-10} cm^2·s^{-1}. Based on the limit of detection of our system, the D_{app} values of the sensitizers we explore in this study are two or more orders of magnitude lower than that of $[Ru(bpy)_2(4,4'\text{-}(PO_3H_2)_2bpy)]$. The difference in D_{app} may be related to the difference in charge between $[Ru(bpy)_2(4,4'\text{-}(PO_3H_2)_2bpy)]$ and the porphyrin sensitizers. Both the Ru(II) and Ru(III) forms of $[Ru(bpy)_2(4,4'\text{-}(PO_3H_2)_2bpy)]$ are charged and water soluble, whereas only the oxidized form of the porphyrin sensitizers is charged. Oxidation of the neutral porphyrin may induce a significant solvent reorganization energy. Also, the hole on the porphyrin cation is ligand centered, whereas on the Ru(III) complexes it is metal centered, which may play some additional role. Efficient hole transport by the sensitizer is crucial to photocurrent generation, so the low D_{app} values of these sensitizers suggest low or negligible photocurrent. As the distance the hole can travel is a function of both D_{app} and τ_r, the order of magnitude increase in recombination time apparently mitigates the low D_{app} values for the porphyrins. The high surface coverages observed for these sensitizers will also help to mitigate a low D_{app}.

On a final note, the porphyrin-sensitized electrodes are active under red light illumination, whereas $[Ru(bpy)_2(4,4'\text{-}(PO_3H_2)_2bpy)]$-sensitized electrodes do not show any photocurrent in the red portion of the spectrum. Most notably the IPCE values for full-spectrum illumination (410 nm long-pass) and for red light illumination (590 nm long-pass) are very similar. Thus, although the actual currents are low, the electrodes use the red photons as well as the rest of the spectrum. The utilization of red light to drive water splitting represents a significant step forward for molecular photoelectrochemical water-splitting systems.

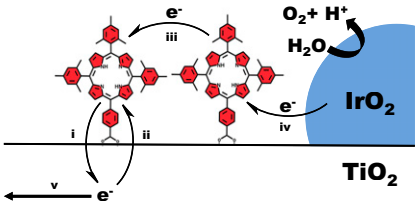

Fig. 4. Selected electron transfer processes in WS-DSPEC: (*i*) injection, (*ii*) recombination, (*iii*) hole transfer, (*iv*) regeneration of oxidized sensitizer, and (*v*) transport to the fluorine-doped tin oxide anode.

Conclusion

In this study we demonstrate a functioning WS-DSPEC, using organic free-base porphyrin sensitizers. The spectral and electrochemical behavior of the free-base porphyrins can be tuned both by the number and by the type of substituents. Fully substituted porphyrins at the meso position exhibit the most red-shifted spectra and are strongly absorbing. Electron-donating substituents that extend the core π system shift E_{pa} to more cathodic values. Although a negative shift of E_{pa} is desirable for injection into TiO_2, it lowers the driving force for oxidation of IrO_2. Although this study has focused mostly on electron-donating aryl substituents, pentafluorophenyl or cyano substituents are electron withdrawing and would provide an alternative pathway for tuning sensitizer energetics.

Despite the variability in their spectral and electrochemical properties, the majority of the porphyrins exhibited significant photocurrent under illumination. Under full visible and red light illumination, the electrodes produced measurable photocurrents and had open-circuit voltages in excess of 1 V, although the photocurrent was lower than that of electrodes sensitized with $[Ru(bpy)_2(4,4'\text{-}(PO_3H_2)_2bpy)]$. The porphyrin sensitizers have lower injection yields and slower hole transport than $[Ru(bpy)_2(4,4'\text{-}(PO_3H_2)_2bpy)]$. The slow hole transport is partially mitigated by an increase in the recombination time.

ACKNOWLEDGMENTS. We thank Prof. Mark Maroncelli for assistance with emission measurements. Work at Pennsylvania State University was supported by the Office of Basic Energy Sciences, Division of Chemical Sciences, Geosciences, and Energy Biosciences, Department of Energy under Contract DE-FG02-07ER15911, and work at Arizona State University was supported as part of the Center for Bio-Inspired Solar Fuel Production, an Energy Frontier Research Center funded by the US Department of Energy, Office of Science, Office of Basic Energy Sciences under Award DE-SC0001016. N.S.M. and D.D.M.-H. thank the National Science Foundation (NSF) for support as graduate fellows under Grant DGE1255832. Instrumentation and facilities used in this project were supported by the Pennsylvania State University Materials Research Institute Nanofabrication Laboratory under NSF Cooperative Agreement ECS-0335765.

1. Swierk JR, Mallouk TE (2013) Design and development of photoanodes for water-splitting dye-sensitized photoelectrochemical cells. *Chem Soc Rev* 42(6):2357–2387.
2. McDaniel ND, Bernhard S (2010) Solar fuels: Thermodynamics, candidates, tactics, and figures of merit. *Dalton Trans* 39(42):10021–10030.
3. McConnell I, Li G, Brudvig GW (2010) Energy conversion in natural and artificial photosynthesis. *Chem Biol* 17(5):434–447.
4. Sundholm D (1999) Density functional theory calculations of the visible spectrum of chlorophyll a. *Chem Phys Lett* 302:480–484.
5. Gouterman M (1978) *The Porphyrins*, ed Dolphin D (Academic, New York), pp 1–165.
6. Li L-L, Diau EW-G (2013) Porphyrin-sensitized solar cells. *Chem Soc Rev* 42(1):291–304.
7. Imahori H, Umeyama T, Ito S (2009) Large π-aromatic molecules as potential sensitizers for highly efficient dye-sensitized solar cells. *Acc Chem Res* 42(11):1809–1818.
8. Giribabu L, Kanaparthi RK (2013) Are porphyrins an alternative to ruthenium(II) sensitizers for dye-sensitized solar cells? *Curr Sci* 104:847–855.
9. Yella A, et al. (2011) Porphyrin-sensitized solar cells with cobalt (II/III)-based redox electrolyte exceed 12 percent efficiency. *Science* 334(6056):629–634.
10. Gao Y, et al. (2013) Visible light driven water splitting in a molecular device with unprecedentedly high photocurrent density. *J Am Chem Soc* 135(11):4219–4222.
11. McAlpin JG, Stich TA, Casey WH, Britt RD (2012) Comparison of cobalt and manganese in the chemistry of water oxidation. *Coord Chem Rev* 256:2445–2452.
12. Du P, Eisenberg R (2012) Catalysts made of earth-abundant elements (Co, Ni, Fe) for water splitting: Recent progress and future challenges. *Energy Environ Sci* 5: 6012–6021.
13. Wiechen M, Berends H-M, Kurz P (2012) Water oxidation catalysed by manganese compounds: From complexes to 'biomimetic rocks'. *Dalton Trans* 41(1):21–31.
14. Fillol JL, et al. (2011) Efficient water oxidation catalysts based on readily available iron coordination complexes. *Nat Chem* 3(10):807–813.
15. Mirzakulova E, et al. (2012) Electrode-assisted catalytic water oxidation by a flavin derivative. *Nat Chem* 4(10):794–801.
16. Youngblood WJ, et al. (2009) Photoassisted overall water splitting in a visible light-absorbing dye-sensitized photoelectrochemical cell. *J Am Chem Soc* 131(3):926–927.
17. Brimblecombe R, Koo A, Dismukes GC, Swiegers GF, Spiccia L (2010) Solar driven water oxidation by a bioinspired manganese molecular catalyst. *J Am Chem Soc* 132(9):2892–2894.
18. Zhao Y, et al. (2012) Improving the efficiency of water splitting in dye-sensitized solar cells by using a biomimetic electron transfer mediator. *Proc Natl Acad Sci USA* 109(39): 15612–15616.
19. Swierk JR, et al. (2014) Photovoltage effects of sintered IrO2 nanoparticle catalysts in water-splitting dye-sensitized photoelectrochemical cells. *J Phys Chem C* 118: 17046–17053.
20. Moore GF, et al. (2011) A visible light water-splitting cell with a photoanode formed by codeposition of a high-potential porphyrin and an iridium water-oxidation catalyst. *Energy Environ Sci* 4:2389–2392.
21. Mishra A, Fischer MKR, Bäuerle P (2009) Metal-free organic dyes for dye-sensitized solar cells: From structure: property relationships to design rules. *Angew Chem Int Ed Engl* 48(14):2474–2499.
22. Ooyama Y, Harima Y (2009) Molecular designs and syntheses of organic dyes for dye-sensitized solar cells. *Eur J Org Chem* 2009:2903–2934.
23. Thompson BC, Fréchet JMJ (2008) Polymer-fullerene composite solar cells. *Angew Chem Int Ed Engl* 47(1):58–77.
24. Dennler G, Scharber MC, Brabec CJ (2009) Polymer-fullerene bulk-heterojunction solar cells. *Adv Mater* 21:1323–1338.
25. Tachan Z, Hod I, Zaban A (2014) The TiO_2–catechol complex: Coupling type II sensitization with efficient catalysis of water oxidation. *Adv Energy Mater*, 10.1002/aenm.201301249.
26. Gouterman M (1961) Spectra of porphyrins. *J Mol Spectrosc* 6:138–163.
27. Watson DF, Marton A, Stux AM, Meyer GJ (2003) Insights into dye-sensitization of planar TiO 2: Evidence for involvement of a protonated surface state. *J Phys Chem B* 107:10971–10973.
28. Kavan L, Grätzel M, Gilbert SE, Klemenz C, Scheel HJ (1996) Electrochemical and photoelectrochemical investigation of single-crystal anatase. *J Am Chem Soc* 118: 6716–6723.
29. Qu P, Meyer GJ (2001) Proton-controlled electron injection from molecular excited states to the empty states in nanocrystalline TiO 2. *Langmuir* 17:6720–6728.
30. Galoppini E, et al. (2002) Long-range electron transfer across molecule-nanocrystalline semiconductor interfaces using tripodal sensitizers. *J Am Chem Soc* 124(26): 7801–7811.
31. Bonhôte P, et al. (1998) Efficient lateral electron transport inside a monolayer of aromatic amines anchored on nanocrystalline metal oxide films. *J Phys Chem B* 102: 1498–1507.
32. Hanson K, et al. (2012) Structure–property relationships in phosphonate-derivatized, Ru IIPolypyridyl dyes on metal oxide surfaces in an aqueous environment. *J Phys Chem C* 116:14837–14847.
33. Swierk JR, McCool NS, Saunders TP, Barber GD, Mallouk TE (2014) Effects of electron trapping and protonation on the efficiency of water-splitting dye-sensitized solar cells. *J Am Chem Soc* 136(31):10974–10982.
34. Bergeron BV, Kelly CA, Meyer GJ (2003) Thin film actinometers for transient absorption spectroscopy: Applications to dye-sensitized solar cells. *Langmuir* 19: 8389–8394.
35. Spellane PJ, Gouterman M, Antipas A, Kim S, Liu YC (1980) Porphyrins. 40. Electronic spectra and four-orbital energies of free-base, zinc, copper, and palladium tetrakis (perfluorophenyl)porphyrins. *Inorg Chem* 19:386–391.
36. Kadish KM, Morrison MM (1976) Solvent and substituent effects on the redox reactions of para-substituted tetraphenylporphyrin. *J Am Chem Soc* 98(11):3326–3328.
37. Helms A, Heiler D, McLendon G (1991) Dependence of electron transfer rates on donor-acceptor angle in bis-porphyrin adducts. *J Am Chem Soc* 113:4325–4327.
38. Fonda HN, et al. (1993) Spectroscopic, photophysical, and redox properties of some meso-substituted free-base porphyrins. *J Phys Chem* 97:7024–7033.
39. Fungo F, Otero L, Durantini EN, Silber JJ, Sereno LE (2000) Photosensitization of thin SnO2 nanocrystalline semiconductor film electrodes with metallodiporphyrin. *J Phys Chem B* 104:7644–7651.
40. Asbury JB, Wang Y-Q, Hao E, Ghosh HN, Lian T (2001) Evidences of hot excited state electron injection from sensitizer molecules to TiO2 nanocrystalline thin films. *Res Chem Intermed* 27:393–406.
41. Martini LA, et al. (2013) Modular assembly of high-potential Zn-porphyrin photosensitizers attached to TiO2 with a series of anchoring groups. *J Phys Chem C* 117: 14526–14533.
42. Brennan BJ, et al. (2013) Comparison of silatrane, phosphonic acid, and carboxylic acid functional groups for attachment of porphyrin sensitizers to TiO2 in photoelectrochemical cells. *Phys Chem Chem Phys* 15(39):16605–16614.